Nondestructive Evaluation of FRP Strengthening Systems Bonded on RC Structures Using Pulsed Stimulated Infrared Thermography, In : Infrared Thermography, Chapter 9

Frédéric Taillade, Marc Quiertant, Karim Benzarti, Jean Dumoulin, Christophe Aubagnac

9

Nondestructive Evaluation of FRP Strengthening Systems Bonded on RC Structures Using Pulsed Stimulated Infrared Thermography

Frédéric Taillade, Marc Quiertant, Karim Benzarti,
Jean Dumoulin and Christophe Aubagnac
Université Paris-Est, IFSTTAR, F-75015 Paris
France

1. Introduction

In civil engineering, strengthening or retrofitting of reinforced concrete (RC) structures by externally bonded Fiber-Reinforced Polymer (FRP) systems is now a commonly accepted and widespread technique (Hollaway, 2010; Quiertant, 2011). However, the use of bonding techniques always implies following rigorous installation procedures (440.2R-08 Committee ACI, 2008; AFGC, 2011; FIB, 2001) and application personnel have to be trained in conformity with installation procedures to ensure both durability and long-term performances of FRP reinforcements. The presence of bonding defects can significantly affect the structural performance and durability of the strengthening systems. Defects have then to be detected, located and evaluated in order to estimate if injection or replacement is needed. In these conditions, conformance checking of the bonded overlays through *in situ* nondestructive evaluation (NDE) techniques is highly suitable. The quality-control program should involve a set of adequate inspections and tests.

Visual inspection and acoustic sounding (hammer tapping) are commonly used to detect delaminations (disbonds) (Fig.1). However, these current practices are unable to provide relevant information about the depth (in the case of multilayered FRP systems) and width of debonded areas and they are not capable of evaluating the level of adhesion between the FRP and the substrate (partial delamination, damage or poor mechanical properties of the polymer adhesive). Adherence properties of FRP systems installed on concrete substrates can be evaluated by conducting on site pull-off adhesion tests on witness panels specifically bonded on test zones (Fig.2).

Consequently, different authors have developed nondestructive methods to assess the quality of the FRP/concrete adhesive bond, based on microwave (Akuthota et al., 2004), acousto-ultrasonic (Ekenel & Myers, 2007), impact-echo (Maerz & Galecki, 2008), shearography (Hung, 2001; Taillade et al., 2011; 2006), infrared thermography (Galietti et al., 2007; Valluzzi et al., 2009) or a coupling of these two latter techniques (Lai et al., 2009; Taillade et al., 2010).

This chapter is devoted to the pulsed stimulated infrared thermography technique applied to the detection and the characterization of the depth and width of adhesion defects (delaminations or adhesive disbonds) of FRP externally bonded on RC structures.

Fig. 1. Inspection with acoustic sounding (hammer tapping).

Fig. 2. Pull-off method.

In a first part, the principle of pulsed stimulated infrared thermography is recalled ; laboratory investigations are then presented in a second part. The laboratory samples contain different defects (with calibrated size and depth) inserted between the concrete substrate and the carbon FRP laminate bonded to its surface. Experiments were conducted in laboratory on the dedicated samples and complementary 2D numerical simulations were also carried-out. Analysis methods of thermograms are presented. Thermal signatures of different geometries of defects are studied in the cases of pulse and square heating thermal excitations. Main advantages of each stimulated technique are discussed in relation to the targeted application. Results from experiments based on long pulse approach are also discussed in details.

In the second part of this chapter, a case study of field application is presented for the proposed method. Inspection is carried-out using a hand-held heating device and an infrared camera. Such a simple technology enables real time NDE in the field with a high efficiency.

2. Principle of pulsed stimulated infrared thermography

For many years, the Pulsed Stimulated Infrared Thermography technique has been used to control aerospace structures, in particular to detect and characterize delaminations in carbon/epoxy composites (Maldague, 2001).

Pulse heating principle consists in heating the surface of the composite during a period τ and measuring the temperature distribution on the sample surface with an infrared camera (Fig.3).

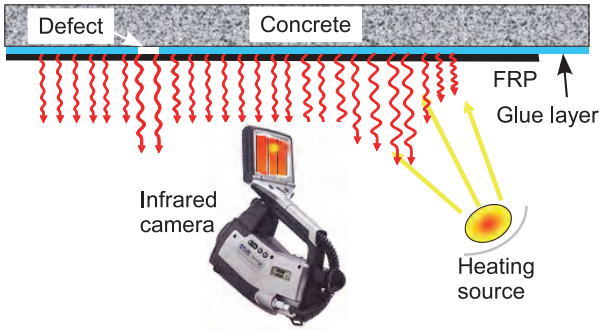

Fig. 3. Principle of stimulated infrared thermography.

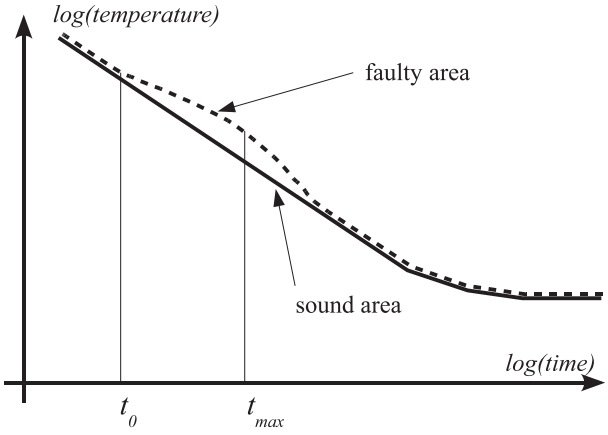

Fig. 4. Thermograms of sound and faulty regions.

Detection and localization of the subsurface defects can then be performed using adequate image analysis approaches (Ibarra-Castanedo et al., 2004). Characterization of the resistive subsurface defects can be achieved by monitoring the emergence of a thermal contrast (Balageas et al., 1987) between sound and faulty areas (Fig.4) after the pulse illumination (thermal relaxation phase). The thermal contrast C_T could be expressed by:

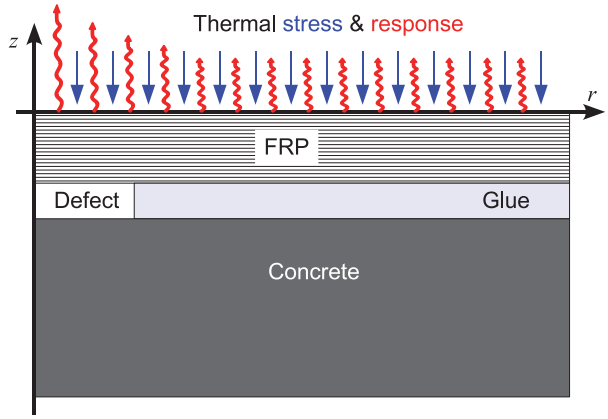

Fig. 5. Axisymmetric finite element model.

$$C_T = \frac{T}{T^{sound}} - 1 \tag{1}$$

where T^{sound} and T are respectively the temperature above sound and faulty regions.

Using the thermal diffusion time concept, hypothesis of heat diffusion in a semi infinite body and assuming the period τ is infinitely short (Dirac pulse), the depth d of the defect can be deduced from the time t_{max} associated to the maximum thermal contrast using the expression:

$$d = \sqrt{\alpha t_{max}} \tag{2}$$

where $\alpha = \lambda / \rho c$ is the thermal diffusivity of the material through the thickness direction with ρ, c and λ are respectively the density, heat capacity and thermal conductivity of the material.

It follows that for defects of same nature but localized at different depths, their localization is based on the detection of thermal contrast appearing at different time on thermal image sequences. For a same thermal solicitation, thermal contrast fades while defect depth increase. So, localization of defects requires to analyze the whole sequence of thermal images acquired during and after thermal solicitation.

3. Finite element simulation for test calibration

In this section, it is proposed to calculate the thermal time response of a sample (carbon FRP / polymer adhesive / concrete) with a bonding defect and subjected to an external heat pulse of finite duration. It is assumed that thermal stress is applied uniformly over the composite surface. To simplify the simulations, an orthotropic behavior is assumed for the FRP material while concrete and polymer adhesive are considered as isotropic. The bonding defects are assumed to be circular areas of finite diameter characterized by a lack of glue (Fig.5). The finite element software enables one to solve the Fourier heat transfer equation:

$$\rho c \frac{\partial T}{\partial t} = div\,(\lambda\ \mathbf{grad}\ T) \tag{3}$$

The FRP reinforcement, which is based on bonded carbon fabrics in this case, is simulated by a definite thickness of carbon/epoxy laminate exhibiting equivalent properties. Thicknesses of the FRP laminate, glue layer and concrete substrate are respectively 2 mm, 0.2 mm and 20 mm. Since a delamination of surface area 6.5 cm^2 is considered as the threshold above which repair should be undertaken (Maerz & Galecki, 2008), various diameters ranging from 10 to 40 mm have been chosen for the bonding defects.

Thermal properties considered in the numerical calculations are given in Table 1 for the different materials.

Table 1. Thermal properties of the materials.

Material	ρ $(kg.m^{-3})$	c $(J.K^{-1}.kg^{-1})$	λ $(W.m^{-1}.K^{-1})$
Epoxy	1200	1200	0.2
Concrete	2300	900	1.8
Composite	1500	850	4.2 along fiber 0.7 perpendicular to the fiber

Figure 6 shows the computed thermal response of the composite surface heated with a thermal flux equal to 1000 $W.m^{-1}$ for 1 s. Time evolutions of the temperature near sound and faulty areas are depicted for defect diameters equal to 20, 30 and 40 mm. Maxima of the thermal contrast (Fig. 7) are respectively observed 9.0 s, 12.5 s and 16.4 s after the end of the heating period, according to the diameter of the defect. Using the composite thermal diffusivity in the transverse direction (perpendicular to the fibers) and equation 2, these characteristic times enable one to estimate an average value of the defect depth, as well as an expanded uncertainty ($k = 2$): $d = 2.7 \pm 0.8$ mm. Although the accuracy is low, it remains in the same range as uncertainties on the thermal properties of materials (typically 20%) and it should be underlined that the thickness of the adhesive layer is not known precisely in most practical cases (typical uncertainty of 30%). We prefer this technique, very simple to implement, rather than the early detection method. Nevertheless, it is to note that the early time detection related to different diameters of the defect is merged at the same short times $t_0 \approx 2.2$ s but it is necessary to apply a threshold of detection factor (Krapez et al., 1994) depending on the noise level of the experiment, in order to assess the depth of the defect with a good accuracy.

To increase the measured thermal contrast, it is possible to apply the thermal flux for a longer period and/or to use a high sensitivity infrared camera (NETD of the order of 25 mK). Moreover, in practice, the second solution is almost unrealistic due to the prohibitive cost of this type of IR camera which is not suitable to field inspections. By increasing pulse duration, the contrast can be enhanced but the maxima of the thermal contrast is delayed (Fig.8) and Equation 2 is not applicable directly any more.

4. Analysis method

Different analysis tools (Balageas et al., 1987; Ibarra-Castanedo et al., 2004; Maldague, 2001) can be used. They are based on techniques of contrast enhancement (increase in the defect signature), thermal images sequence decomposition on basis (data compression) and image segmentation (localization of defects on thermal images).

A first approach to reduce the number of thermal images to be analyzed in a sequence (Ibarra-Castanedo et al., 2004) consists in using frequency analysis tools. The Fourier

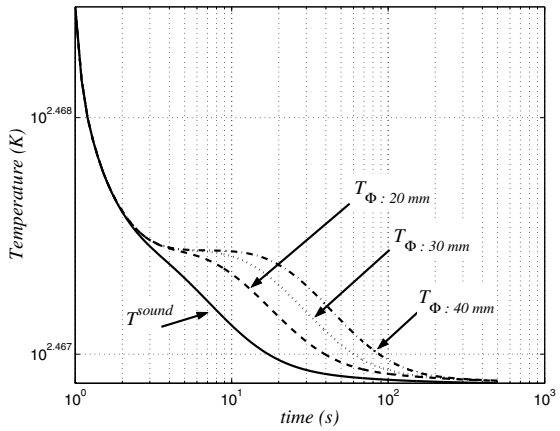

Fig. 6. Thermograms of sound and faulty regions for three defect diameters.

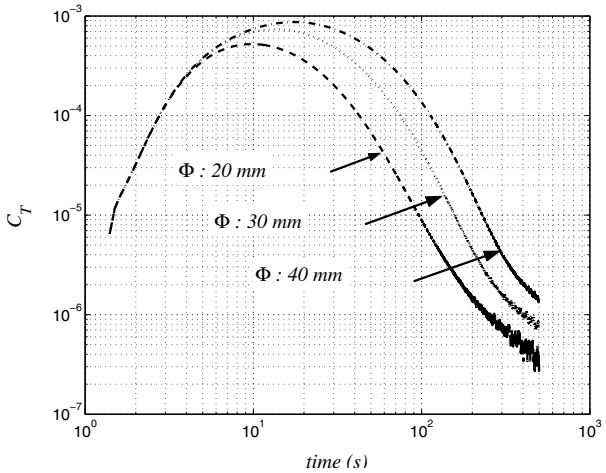

Fig. 7. Thermal contrast simulation for three defect diameters.

transform (Equ.4) is applied to temporal evolution of each pixel of the thermal image ($T(t)$):

$$F_n = \Delta t \sum_{m=0}^{N-1} T(m\Delta t) exp(-j2\pi n/N) \tag{4}$$

where Δt is the sampling time, F_n is the complex image of the n^{th} frequency and N the maximum number of the frequencies.

Magnitude and phase maps calculated are then analyzed to locate defects.

Another approach is based on Singular Value Decomposition (SVD) which is an interesting tool for the extraction of the spatial and temporal information from a thermographic matrix

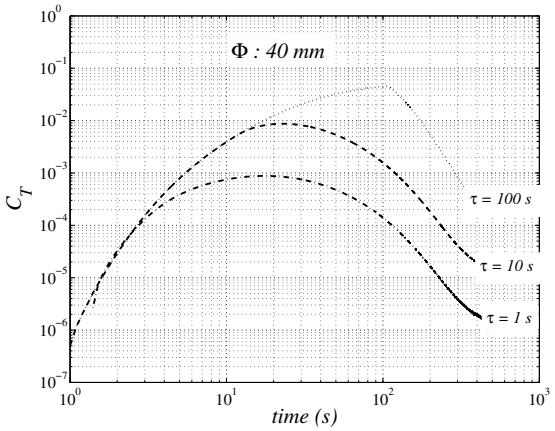

Fig. 8. Thermal contrast simulation for three thermal flux durations τ and 40 mm defect diameter.

in a compact or simplified manner (Rajic, 2002). The SVD of a $M \times N$ matrix A ($M > N$) can be calculated as follows:

$$A = U \sum V^T \tag{5}$$

where U is a $M \times N$ orthogonal matrix, $\sum$ is a diagonal $N \times N$ matrix (with the singular values of A in the diagonal), and V^T is the transpose of a $N \times N$ orthogonal matrix (characteristic time).

Hence, to apply the SVD to thermographic data, the 3D thermogram matrix representing time and spatial variations has to be reorganized as a 2D $M \times N$ matrix A. This can be done by rearranging the thermograms for every time as columns in A, in such a way that time variations will occur column-wise while spatial variations will occur row-wise.

Under this configuration, the columns of U represent a set of orthogonal statistical modes known as Empirical Orthogonal Functions (EOF) that describe the spatial variations of data. On the other hand, the Principal Components (PC), which represent time variations, are arranged row-wise in matrix V^T. The first EOF will represent the most characteristic variability of the data; the second EOF will contain the second most important variability, and so on. Usually, original data can be adequately represented with only a few EOF. Typically, a 1,000 thermal images sequence can be replaced by 5 to 10 EOF and analyzed to locate defects.

When the defect is located (spatially) in the image sequence using one of the previous methods, the method can be refined in order to improve the determination of the defect depth, i.e. (i) to be insensitive to the material anisotropy in terms of thermal diffusivity (Krapez et al., 1994) if we determine the early detection time t_0 (Fig.4) and (ii) to take the non uniformity of the heat flux into account (Krapez et al., 1992). As shown in figure 8, in the case of a finite pulse duration τ, equation 2 must be modified.

The first order correction consists in moving the time scale origin toward the pulse barycenter (Degiovanni, 1987). Moreover, in the case of an infinitely extended defect located in a homogeneous medium, Krapez (Krapez, 1991) has proposed an abacus to apply a correction and take the pulse duration into account (Fig.9).

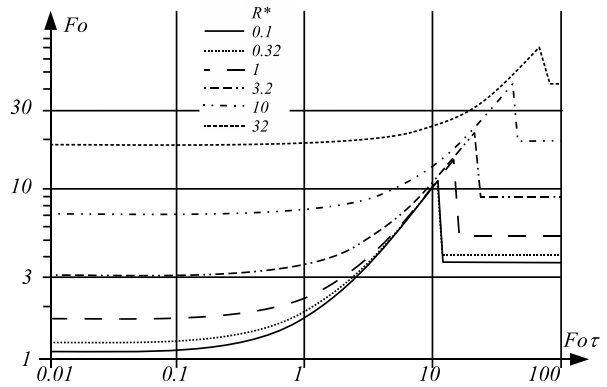

Fig. 9. Variation of the Fourier number F_0 *vs.* the pulse duration for different thermal resistances of the defect.

This abacus (Fig.9) gives the variation of the Fourier number F_0 ($F_0 = \alpha t_{max}/d^2$) as a function of the pulse Fourier number $F_{0\tau}$ ($F_{0\tau} = \alpha\tau/d^2$) for various thermal resistances of the defect R^*, where R^* is the ratio between the discontinuity resistance of the defect R and the resistance of the front layer ($R^* = R/\,(d/\lambda)$).

Although the composite can not be considered as an isotropic material and defects have a finite size, it is proposed to use this abacus in our case in order to improve the estimation of the defect's depth.

Equation 2 is then used in a first approximation to estimate the depth of the defect d. This depth enables one to compute the different parameters R^* and $F_{0\tau}$ used in the abacus (Fig.9). Finally, a value of F_0 is determined and we use it to improve the depth estimation and so on (Fig.16):

$$d' = \sqrt{\frac{\alpha t_{max}}{F_0}} \tag{6}$$

where d' is the new value of depth.

5. Experimentations

Laboratory tests have been carried out to evaluate the performance of the proposed NDE method. A concrete slab ($400 \times 300 \times 15\ mm^3$) has been manufactured and externally reinforced by three superimposed layers of pultruded FRP plates (thickness of 1.2 *mm*) with intermediate glue layers of thickness 1 *mm*, as shown in figure 10. Bonding defects were simulated by locally replacing the adhesive by polytetrafluoroethylene (PTFE) discs (0.5 *mm* thick), placed either between the concrete surface and the lower FRP plate, or between two adjacent FRP layers. The final specimen contains discs of three different diameters (10, 20 and 30 *mm*), located at three different depths (1.2, 3.4 and 5.6 *mm*).

The surface of the specimen was heated during 50 *s* using a flexible electric cover (electric power is about 1000 *W* and the surface is $1 \times 0.9\ m^2$). To visualize the temperature of the sample surface during the cooling phase after external heating, we used an infrared camera which produces images of 320×240 pixels and composed of uncooled microbolometer

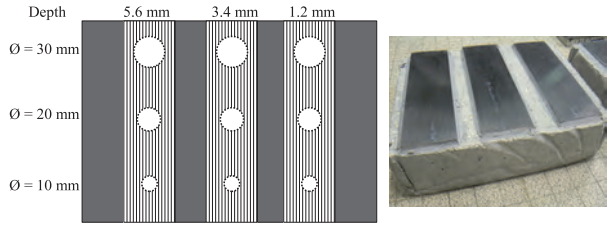

Fig. 10. Concrete slab reinforced with bonded FRP plates (3 superimposed layers) and containing calibrated defects.

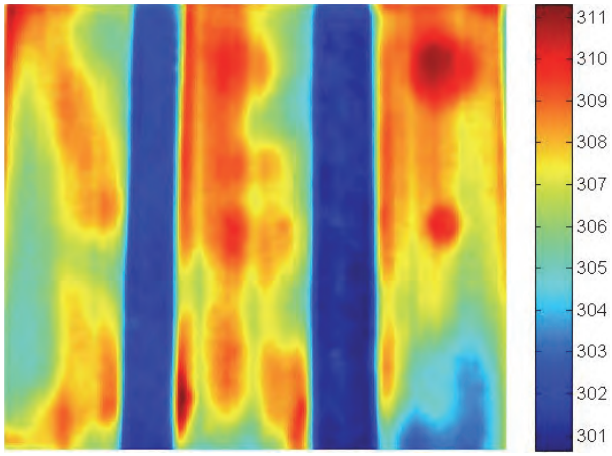

Fig. 11. Thermal image at the beginning of thermal relaxation.

detectors allowing to see temperature differences as low as 80 mK in the range from $-40^{\circ}C$ to $+2,000^{\circ}C$. The spectral response is comprised between 7.5 and 13 μm.

Figures 11 and 12 show thermal images of the sample at the beginning of the thermal relaxation and 52 s after the end of the heating stage. On these figures, we notice the non homogeneity of the heating.

Using SVD method to analyze the sequence of acquired thermal images, one can select only few images to localize the defects (Fig.13). Furthermore, SVD method in that case partly corrects effects of the non homogeneity of the previous heating.

The thermograms (Fig.14) and the thermal contrast (Fig.15) are computed above the larger defect (diameter = 30 mm). The maximum contrast appears 7 s, 33 s and 120 s after the end of the heating respectively to the depth. Using equations (2) and (6) iteratively, it is possible to retrieve the defect's depth with a good accuracy in the three cases considered here.

Taking the thermal diffusivity perpendicular to the FRP into account, and after some iterations (Fig.16), the depth of the defects and its expanded uncertainty ($k = 2$) were estimated to 1.2 ± 0.2 mm, 3.3 ± 0.3 mm and 6.3 ± 0.3 mm which can be compared to the actual depth values of 1.2, 3.4 and 5.6 mm. Globally, a fairly good agreement was obtained. However, it is

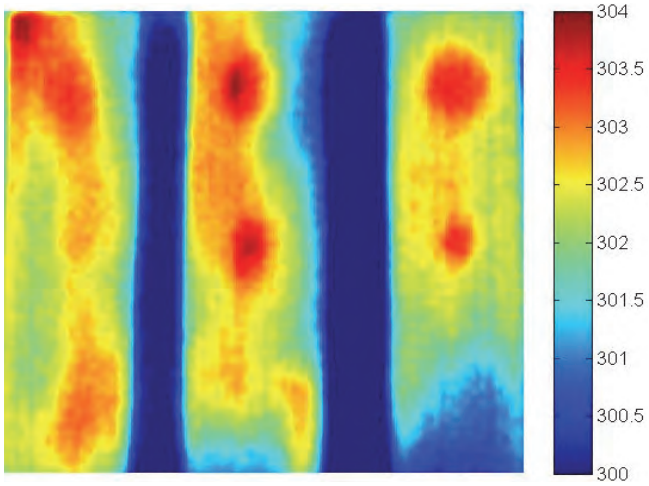

Fig. 12. Thermal image 52 *s* after the end of the heating stage.

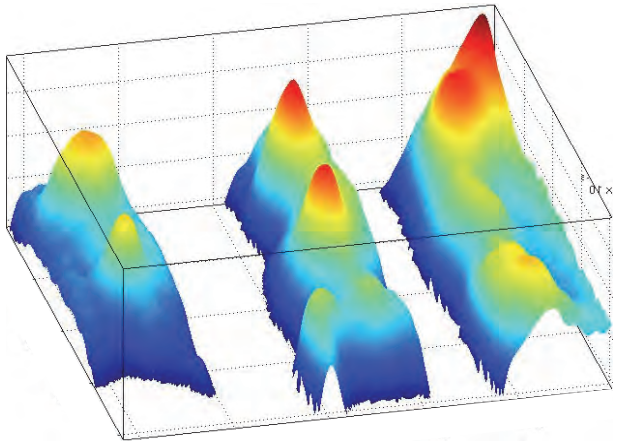

Fig. 13. 3D view of EOF map obtained with SVD method.

to note that an increased deviation was observed for the defect depth of 5.6 *mm*, since in this case measured temperature values were very close to the ambient noise.

6. Field inspection - a case study

In this part, the feasibility of the thermographic method for routine inspection of strengthened concrete structures is illustrated through a case study conducted on an existing RC structure. The field test presented in this section only focuses on the detection of bonding defects. Evaluation of the depths of localized defects was not performed here.

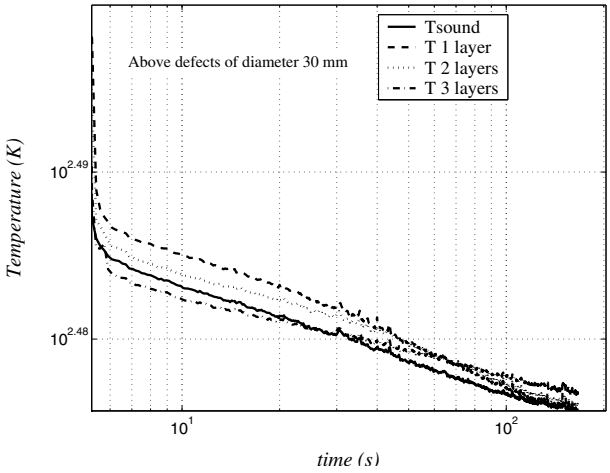

Fig. 14. Experimental thermograms of sound (solid line) and faulty regions above the larger defects (dashed line for a depth of 1.2 *mm*, dotted line for a depth of 3.4 *mm* and dash-dot line for a depth of 5.6 *mm*).

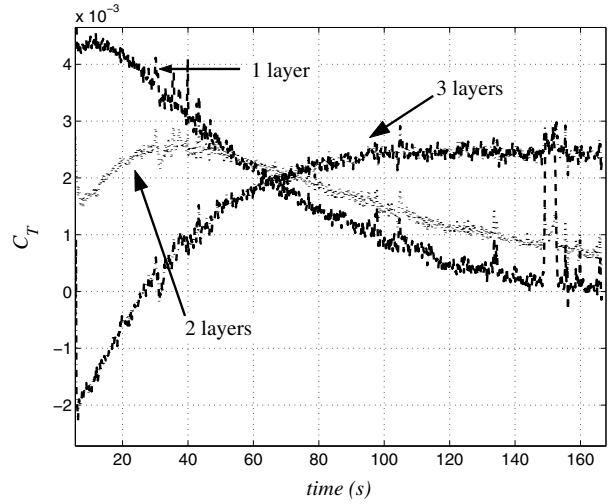

Fig. 15. Thermal contrast *vs.* computed time for regions above the larger defects (dashed line for a depth of 1.2 *mm*, dotted line for a depth of 3.4 *mm* and dash-dot line for a depth of 5.6 *mm*).

6.1 Description of the bridge and repair works

The bridge under study is located near Besançon in France, over the Doubs river. It was built in the 60ies. The bridge consists in three distinct and independent sections, i.e, 2 access spans and a main central structure. The latter is divided itself into three spans, respectively 29, 54 and 29 m long, and composed of two box-girders made of prestressed concrete.

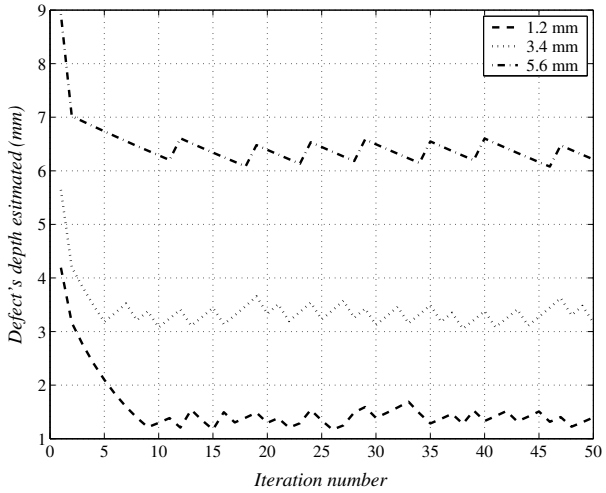

Fig. 16. Iterative estimation of the defect's depth (dashed line for a depth of 1.2 *mm*, dotted line for a depth of 3.4 *mm* and dash-dot line for a depth of 5.6 *mm*).

Fig. 17. View of the bridge under consideration; FRP repaired zones correspond to the white parts on the girders.

A visual inspection conducted in the 90ies revealed extensive transverse cracking of lower slabs of box-girders at mid-span. Such a deterioration was mainly attributed to an inadequate of the thermal gradients consideration in the initial design and to a lack of the inter-element continuity of longitudinal prestressing in lower slabs.

In order to prevent brittle failure at mid-span, it was decided to repair the cracked box-girders by bonding carbon fibre sheets according to the wet lay-up process (onsite impregnation). A recalculation of the structure was performed in order to optimize the repair design with respect to the shear stress distribution. Finally, composite reinforcements were installed at the outer side of the web of girders as shown in figure 17.

Fig. 18. Inspection operations.

6.2 Thermographic inspection of the FRP repairs

The first operational evaluation of the innovative thermographic method was accomplished during the inspection of the CFRP installation. The *in situ* inspection procedure is based on the use of an uncooled infrared camera coupled with a hand-held thermal excitation device consisting of an infrared lamp or an electric cover.

Such a simple set-up offers a fully portable real-time assessment system. The main difficulty of the inspection was the accessibility to the FRP bonded areas, which was resolved by using a truck mounted lift-platform (Fig. 18).

Figure 19 shows the geometrical configuration of the controlled area. The thermal solicitation is imposed by heating the FRP surface with an infrared lamp. Two examples of detected defects are presented in figure 20. The top image shows a wrapping defect and the bottom

Fig. 19. Shematic representation of the survey area by active infrared thermography.

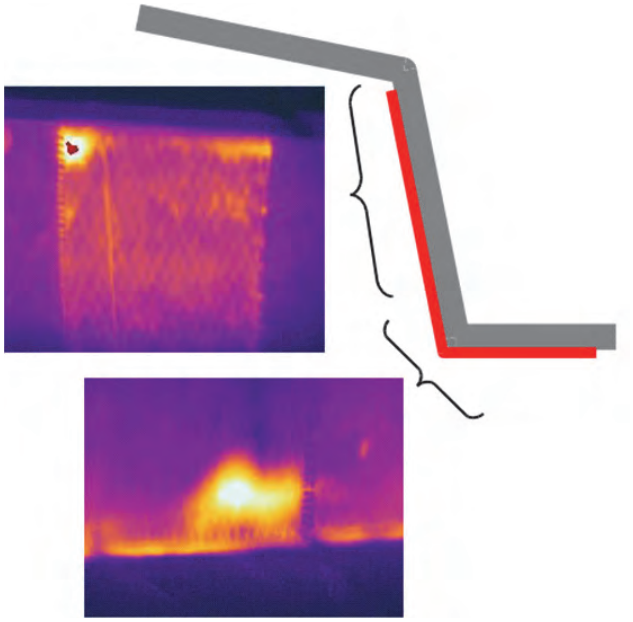

Fig. 20. Thermal images showing defect on bonded CFRP wrap.

image a gluing defect. These two small debonds were confirmed afterwards by hammer tapping.

7. Conclusion

In this paper, basic principles of the pulsed stimulated infrared thermography technique used for NDE of bonded overlays are briefly recalled. A finite element simulation of the thermal time response of bonding defects on a concrete sample reinforced by externally bonded FRP makes it possible to calibrate this NDE technique for this particular application. Moreover, a theoretical analysis of the thermograms is developed in order to quantify the defect depth. Besides, a laboratory evaluation, performed on FRP-strengthened concrete sample containing calibrated defects, has demonstrated the effectiveness of the method for detecting and assessing the depth of the bond defects. Defects were located between concrete and external FRP reinforcements or between two layers of FRP.

Thermography offers a simple method with real time and full field imaging capabilities. Moreover, hand portability of the thermal imaging equipment, including the heating source, is well adapted to field application. Furthermore, feasibility of the thermographic inspection method into the field was demonstrated during the inspection of a recently CFRP strengthened bridge. In this last validation test, only qualitative evaluation of the adhesive bond was performed (detection of the bonding defects). Based on satisfactory laboratory and field results, it is the author's point of view that a coupling of the two methods (pulsed stimulated infrared thermography and analysis of the thermograms) will offer an effective NDE tool for the evaluation of FRP strengthening systems bonded on concrete structures.

8. References

440.2R-08 Committee ACI (2008). Guide for the design and construction of externally bonded FRP systems for strengthening concrete structures, *Technical report*, ACI, Michigan (US).

AFGC (2011). Réparation et renforcement des structures en béton au moyen des matériaux composites, *Technical report*, Bulletin scientifique et technique de l'AFGC. in French.

Akuthota, B., Hughes, D., Zoughi, R., Myers, J. & Nanni, A. (2004). Near-field microwave detection of disbond in carbon fiber reinforced polymer composites used for strengthening cement-based structures and disbond repair verification, *Journal of Materials in Civil Engineering* 16(6): 540–546.

Balageas, D., Déom, A. & Boscher, D. (1987). Characterization and nondestructive testing of carbon-epoxy composites by a pulsed photothermal method, *Materials Evaluation* 45(4): 461.

Degiovanni, A. (1987). Correction de longueur d'impulsion pour la mesure de la diffusivité thermique par méthode flash, *International Journal of Heat and Mass Transfert* 30(10): 2199–2200.

Ekenel, M. & Myers, J. (2007). Nondestructive evaluation of RC structures strengthened with FRP laminates containing near-surface defects in the form of delaminations., *Science and Engineering of Composite Materials.* 14(4): 299–315.

FIB, T. G. . (2001). Externally bonded FRP reinforcement for RC structures, *Technical Report 14*, Fib bulletin 14, Lausanne, Switzerland.

Galietti, U., Luprano, V., Nenna, S., Spagnolo, L. & Tundo, A. (2007). Non-destructive defect characterization of concrete structures reinforced by means of FRP, *Infrared Physics & Technology* 49: 218–223.

Hollaway, L. (2010). A review of the present and future utilisation of FRP composites in the civil infrastructure with reference to their important in-service properties., *Construction and Building Materials* 24(12): 2419–2445.

Hung, M. Y. Y. (2001). Shearography and applications in nondestructive evaluation of structures, *Proceedings of the International Conference on FRP Composites in Civil Engineering (CICE 2001)*, pp. 1723–1730.

Ibarra-Castanedo, C., González, D., Klein, M., Pilla, M., Vallerand, S. & Maldague, X. (2004). Infrared image processing and data analysis, *Infrared Physics* 46: 75–83.

Krapez, J.-C. (1991). *Contribution à la caractérisation des défauts de type délaminage ou cavité par thermographie stimulée*, PhD thesis, Ecole Centrale de Paris.

Krapez, J.-C., Boscher, D., Delpech, P., Déom, A., Gardette, G. & Balageas, D. (1992). Time-resolved pulsed stimulated infrared thermography applied to carbon-epoxy non destructive evaluation, *Quantitative Infrared Thermography (QIRT 92)*.

Krapez, J.-C., Lepoutre, F. & D. Balageas, . (1994). Early detection of thermal contrast in pulsed stimulated thermography, *8th International Topical Meeting on Photoacoustic and Photothermal Phenomena*.

Lai, W. L., Poon, S. C. K. C. S., Tsang, W. F., Ng, S. P. & Hung, Y. Y. (2009). Characterization of flaws embedded in externally bonded CFRP on concrete beams by infrared thermography and shearography, *Journal of Nondestructive Evaluation* 28(1): 27–35.

Maerz, N. H. & Galecki, G. (2008). Preservation of missouri transportation infrastructures: Validation of FRP composite technology, *Technical Report Volume 4 of 5 Non-Destructive Testing of FRP Materials and Installation, Gold Bridge*, Prepared by Missouri S&T and Missouri Department of Transportation.

Maldague, X. P. V. (ed.) (2001). *Theory and practice of infrared technology for non-destructive testing*, John Wiley & sons Inc.

Quiertant, M. (2011). *Strengthening concrete structures by externally bonded composite materials*, ISTE-Wiley, chapter Chapter 23. of Organic Materials for Sustainable Construction, pp. 503–525.

Rajic, N. (2002). Principal component thermography for flaw contrast enhancement and flaw depth characterisation in composite structures, *Composite Structures* 58: 521–528.

Taillade, F., Quiertant, M., Benzarti, K. & Aubagnac, C. (2010). Shearography and pulsed stimulated infrared thermography applied to a nondestructive evaluation of FRP strengthening systems bonded on concrete structures, *Construction and Building Materials* 25(2): 568–574.

Taillade, F., Quiertant, M., Benzarti, K., Aubagnac, C. & Moser, E. (2011). Shearography applied to the non destructive evaluation of bonded interfaces between concrete and CFRP overlays, *European Journal of Environmental and Civil Engineering* 15(4): 545–556.

Taillade, F., Quiertant, M. & Tourneur, C. (2006). Nondestructive evaluation of FRP bonding by shearography, *Proceeding of the Third International Conference on FRP Composites in Civil Engineering (CICE 2006)*, Miami, Florida, US, pp. 327–330.

Valluzzi, M. R., Grinzato, E., Pellegrino, C. & Modena, C. (2009). IR thermography for interface analysis of FRP laminates externally bonded to RC beams, *Materials and Structures* 42(1): 25–34.